Transport in carbon nanotubes: Two-level SU(2) regime reveals subtle competition between Kondo and intermediate valence states

C. A. Büsser, E. Vernek, P. Orellana, G. A. Lara, E. H. Kim, A. E. Feiguin, E. V. Anda, and G. B. Martins

Phys. Rev. B **83**, 125404 — Published 14 March 2011

DOI: 10.1103/PhysRevB.83.125404

Transport in Carbon Nanotubes: 2LSU(2) regime reveals subtle competition between Kondo and Intermediate Valence states

C. A. Büsser,[1,2] E. Vernek,[3] P. Orellana,[4] G. A. Lara,[5] E. H. Kim,[6] A. E. Feiguin,[2] E. V. Anda,[7] and G. B. Martins[1,*]

[1]*Department of Physics, Oakland University, Rochester, MI 48309, USA*
[2]*Dept. of Physics and Astronomy, University of Wyoming, Laramie, WY 82071, USA*
[3]*Instituto de Física - Universidade Federal de Uberlândia - Uberlândia, MG 38400-902 - Brazil*
[4]*Departamento de Física, Universidad Católica del Norte, Casilla 1280, Antofagasta, Chile*
[5]*Departamento de Física, Universidad de Antofagasta, Casilla 170, Antofagasta, Chile*
[6]*Department of Physics, University of Windsor, Windsor, ON, N9B 3P4, Canada*
[7]*Departamento de Física, Pontifícia Universidade Católica do Rio de Janeiro, 22453-900, Brazil.*

In this work, we use three different numerical techniques to study the charge transport properties of a system in the two-level SU(2) (2LSU2) regime, obtained from an SU(4) model Hamiltonian by introducing orbital mixing of the degenerate orbitals via coupling to the leads. SU(4) Kondo physics has been experimentally observed, and studied in detail, in Carbon Nanotube Quantum Dots. Adopting a two molecular orbital basis, the Hamiltonian is recast into a form where one of the molecular orbitals decouples from the charge reservoir, although still interacting capacitively with the other molecular orbital. This basis transformation explains in a clear way how the charge transport in this system turns from double- to single-channel when it transitions from the SU(4) to the 2LSU2 regime. The charge occupancy of these molecular orbitals displays gate-potential-dependent occupancy oscillations that arise from a competition between the Kondo and Intermediate Valence states. The determination of whether the Kondo or the Intermediate Valence state is more favorable, for a specific value of gate potential, is assessed by the definition of an energy scale T_0, which is calculated through DMRG. We speculate that the calculation of T_0 may provide experimentalists with a useful tool to analyze correlated charge transport in many other systems. For that, a current work is underway to improve the numerical accuracy of its DRMG calculation and explore different definitions.

PACS numbers: 73.23.Hk, 72.15.Qm, 73.63.Kv

I. INTRODUCTION

Interest in charge transport properties of carbon nanotubes (CNT)[1] has grown consistently in the last few years, in part because of their possible applications as single electron transistors (SETs),[2] as well as their possible use in molecular computing.[3] A CNT SET can be manufactured by coupling a CNT quantum dot (QD) to metal leads[2]. In this case, below a certain characteristic temperature T_K, the Kondo effect[4] was first observed in CNT QDs in 2000.[5] Further investigation showed that the main difference between the Kondo effect in CNT QDs, and the same effect in other nano-structures, comes from the degeneracy of the orbital (chiral) states of the CNT QD.[6] Effectively, while in the one hand the Kondo effect in, e.g., a lateral semiconducting QD is associated to the screening of a localized magnetic moment (in general, with SU(2) symmetry) by the spin density of the conduction electrons, in the other hand, in a CNT QD the two degenerate orbital states with different chirality (usually referred to as a pseudospin), together with the intrinsic spin degree of freedom, give rise to the so-called SU(4) Kondo effect. This exotic state has been recently studied both experimentally[6] and theoretically.[7–10] Some of the many particular characteristics of the SU(4) Kondo effect are (i) a larger Kondo temperature than in the SU(2) case, (ii) Kondo effects at two different fillings, namely, quarter-filling and half-filling, with diverse properties,[10] (iii) a rich behavior under magnetic field,[11] (iv) perfect entanglement of spin and orbital degrees of freedom,[6] among others.

Another interesting regime in the SU(4) Kondo Hamiltonian can be obtained by the gradual 'mixing' of orbital states at the tunneling barriers, through tunneling that effects a flip in the pseudospin of the electron [henceforth, pseudospin conserving tunneling occurs through a matrix element t', and non-conserving through t'', see Fig. 1(a)]. When this mixing is total (i.e., $t''/t' = 1$), one reaches the so-called two-level SU(2) (2LSU2) state.[9,10] One constraint associated to the use of a CNT QD to observe SU(4) Kondo physics is the lack of control over the parameters of the system (intra- and inter-orbital Coulomb repulsions U and U', respectively, and couplings to leads), making it impossible to freely navigate from the SU(4) to the 2LSU2 state. In contrast, recent advances in the lithography of semiconducting lateral QDs have allowed greater control over capacitively coupled double quantum dot (DQD) systems connected to independent leads.[12] In reality, it was in a DQD system that the first claim of observation of the SU(4) Kondo effect was made.[13] As long as progress in this field continues to be made, it is not unlikely that the 2LSU2 regime will be accessible to experimental probing in the near future. Indeed, in the same way that the SU(4) regime has been shown to be quite robust regarding a difference between U and U', and some mixing of the orbital states (although *strict* SU(4) symmetry only occurs at one point in parameter space),[8] most of the relevant phenomena described here for the 2LSU2 state are shown to survive a deviation of t''/t' from 1. It is for that reason that we elect to use the terminology SU(4) and 2LSU2 *regimes*, since as far as experiments go, their characteristic properties do not seem to be restricted to the corresponding point in parameter space (we choose to refer to these specific points as SU(4) and 2LSU2 *states*).

In this paper, using three different numerical techniques, namely the Numerical Renormalization Group (NRG),[14] the Density Matrix Renormalization Group (DMRG),[15] and the Logarithmically Discretized Embedded Cluster Approximation (LDECA),[16] we analyze in detail the opposite end of the SU(4) regime, the above mentioned 2LSU2 regime.[9,10] Using the notation defined above, the difference between the SU(4) and 2LSU2 regimes resides in the value of the ratio $\nu = t''/t'$: $\nu = 0$ corresponds to the SU(4) regime (no orbital mixing) and $\nu = 1$ to the 2LSU2 regime (total orbital mixing). The motivations for the study presented here are four-fold: First, in previous work by two of the current authors, a charge discontinuity and a transition from a $2G_0$ to G_0 maximum conductance was observed in the 2LSU2 regime (G_0 is the conductance quantum).[10,17] Second, in these same works, a fine-structure of conductance peaks ($2G_0$ high and positioned at and around the particle-hole (p-h) symmetric point) was observed for parameter values in the 2LSU2 regime, superimposed over a flat background of height G_0. Third, a slave boson analysis of the local density of states (LDOS) showed a discontinuous change of the Kondo peak *at* the 2LSU2 regime.[9] All these three points mentioned above were never fully explained, some of them being thought to be related to convergence problems in the numerical methods used.[18] Here, we will show that this is not the case, and that they are associated to a band-decoupling at the 2LSU2 state and to an interesting competition between two distinct many-body ground states. Finally, the above mentioned advances in manufacturing of capacitively coupled DQDs may open the doors for the experimental analysis of the regime theoretically discussed here. Note that to facilitate the connection and comparison with previous work by some of the authors, we will keep referring to the system under study as a CNT QD, although the regime of parameters to be analyzed ($\nu \lesssim 1$) may not be accessible to CNT QDs.

Another interesting aspect of the results presented here is that the points mentioned above (charge discontinuity, change from double- to single-channel charge transport, fine structure of the conductance, and discontinuity in the LDOS Kondo peak) can be more easily understood after a change of basis from 'atomic' to 'molecular' orbitals (AOs to MOs) is applied. Indeed, QDs have been dubbed 'artificial atoms', and systems of two or more coupled QDs have been dubbed 'artificial molecules'. When the phenomena being analyzed depend more on the properties of quantum states involving more than one QD (a 'molecular orbital'), a change of basis from local states (individual QDs) to extended states, involving two or more QDs, should be done to help understand the phenomena being observed.[19] In this work, the authors will present a situation where this change of basis is crucial for the understanding of the numerical results.

This work is divided as follows: Section II briefly presents a description of the model Hamiltonian, and the regime of parameters to be analyzed. In addition, a brief description of the band decoupling occurring at the 2LSU2 state is described by introducing molecular orbitals (a detailed description is provided in Appendix A). Section III presents charge vs. gate voltage results obtained with DMRG and NRG, at zero temperature. Charge oscillations in the MOs, as a function of gate voltage, are in perfect agreement between the two techniques. The NRG results are extended to finite temperatures, determining the energy scale of the phenomena relevant for the V_g-dependent charge oscillations. In addition, to facilitate the discussion of the results, the idea of an effective gate potential V_g^* is introduced. Section IV presents LDECA results for charge, conductance, and spin- and charge-fluctuations, *away* from the 2LSU2 point, in good qualitative agreement with the DMRG results. Section V presents a discussion of the origin of the V_g-dependent charge oscillations observed in the MOs, and, more importantly, an explanation of its dependence on the coupling of the CNT QD to the leads. These charge oscillations in the MOs reveal a subtle competition between two many-body states, namely, the Kondo state and the Intermediate Valence state. A simple way of quantifying this competition is obtained by using DMRG simulations to calculate the energy T_0 of the system for a wide window of gate potential V_g (see Eq. (12) for its definition and discussion thereafter). In addition, the DMRG calculation of T_0 for the single impurity Anderson Model is compared to the Kondo temperature expression derived by Haldane.[20] A finite size scaling of the DMRG results shows that T_0 tends to Haldane's expression in a narrow window around the p-h symmetric point, leading the authors to speculate that the definition and numerical calculation of T_0 may be helpful to study correlated charge transport for a broad region of gate potential, including the Kondo and Intermediate Valence regimes. Section VI presents our conclusions. Appendix A presents details of the basis transformation that results in the band decoupling essential to understand the properties of the 2LSU2 regime, and Appendix B shows results for the non-interacting model ($U = U' = 0.0$).

II. HAMILTONIAN AND MOLECULAR ORBITALS

A. Model Hamiltonian

The SU(4) Hamiltonian used to model a CNT QD (or a capacitively coupled DQD)[13] coupled to metallic leads is given by

$$H_{\rm tot} = H_{\rm mb} + H_{\rm band} + H_{\rm hyb}, \tag{1}$$

$$H_{\rm mb} = \sum_{\sigma;\lambda=\alpha,\beta} \left[\frac{U}{2} n_{\lambda\sigma} n_{\lambda\bar{\sigma}} + V_g n_{\lambda\sigma} \right] + U' \sum_{\sigma\sigma'} n_{\alpha\sigma} n_{\beta\sigma'}, \tag{2}$$

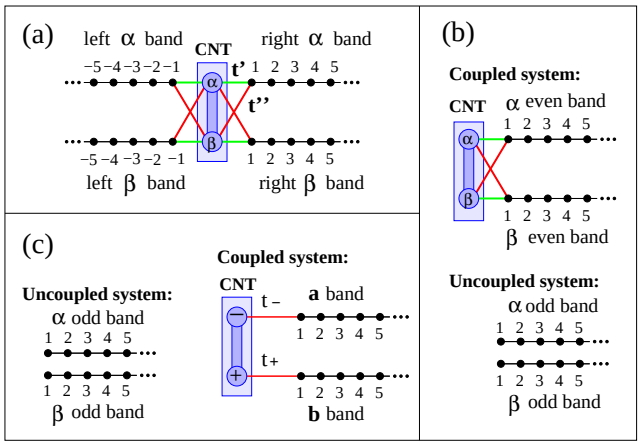

FIG. 1: (Color online) (a) Schematics of the *full* system studied in this work, representing either a CNT (in which case α and β stand for the orbital (chiral) levels of the CNT), or a capacitively coupled DQD (in which case α and β stand for two QDs that are coupled to each other only through a long range Coulomb interaction). In either case, the orbital levels of the QDs are each coupled to its own independent charge reservoir, through hopping t' (gray (green) line). Coupling to a reservoir with opposite quantum number occurs through hopping t'' (black (red) line). The SU(4) state is achieved for $t''=0$, and the 2LSU2 state is achieved for $t''=t'$. (b) Schematics of the usual left-right symmetry transformation that, in this case, decouples two bands from the interacting levels. (c) Final system, obtained after the second symmetry transformation (see text). Now, the MOs $|+\rangle$ and $|-\rangle$ are coupled to bands through hoppings t_+ and t_- that depend on the ratio $\nu = t''/t'$. For $\nu = 1$ (2LSU2 state), level $|-\rangle$ decouples from the electron reservoir, staying coupled to the rest of the system through its many-body capacitive coupling to level $|+\rangle$.

$$H_{\rm band} = t \sum_{\lambda=\alpha,\beta} \sum_{i=1,\sigma}^{\infty} (c^{+}_{\lambda i\sigma} c_{\lambda i+1\sigma} + c^{+}_{\lambda -i\sigma} c_{\lambda -i-1\sigma}) + \text{H.c.}, \quad (3)$$

$$H_{\rm hyb} = \sum_{\lambda,\lambda'=\alpha,\beta,\sigma} t_{\lambda\lambda'} \left[d^{\dagger}_{\lambda\sigma} c_{\lambda' \pm 1\sigma} + \text{H.c.} \right]. \quad (4)$$

Our unit of energy is t, and all results were obtained for $U = U' = t$. Note that this Hamiltonian is p-h symmetric for $V_g/U = -1.5$. $H_{\rm mb}$ contains all the many-body terms in the system; more specifically, $\lambda = \alpha, \beta$ are two degenerate orbitals associated to the wrapping mode (clockwise or anticlockwise) of the electron propagation along the axial direction of the CNT, while $d_{\alpha\sigma}$ ($d_{\beta\sigma}$) annihilates an electron with spin σ in the α (β) orbital in the CNT QD and $c_{\lambda i\sigma}$ annihilates an electron with spin σ in the i-th site of the $\lambda = \alpha$ or β channel for $i > 0$ or $i < 0$ [right or left leads, respectively, see Fig. 1(a)]. Therefore, each lead has two bands, also named α and β, after the notation used for the orbital levels in the QD. Justifications for this assumption are given elsewhere.[10] It is important to stress that the CNT QD is coupled to two independent metallic leads on each side (at left and right), which have the same chiral states as the CNT QD (and therefore the same quantum numbers). Equations (3) and (4) describe the leads and their coupling to the QD, respectively. More specifically, $t_{\alpha,\alpha} = t_{\beta,\beta} = t'$ and $t_{\alpha,\beta} = t_{\beta,\alpha} = t''$. To explore the 2LSU2 regime, we wish to perform numerical calculations for $\nu \lesssim 1$. Following Ref. 9, we will define $\phi = \tan^{-1}(\nu)$, with which the hoppings between the QD and leads can be rewritten as $t'' = t_0 \sin(\phi)$ and $t' = t_0 \cos(\phi)$, where t_0 is kept constant, and t' and t'' are indicated in Fig. 1(a). Using this definition ensures that a constant coupling $\Gamma = 2\pi\rho_0 (E_F) t_0^2$ (where ρ_0 is the reservoir's DOS at the Fermi energy) between the QD and the charge reservoirs is kept constant, while the ratio ν varies. Note that $\nu = 0$ ($t'' = 0$ and $t' = t_0$), the pure SU(4) state, implies $\phi = 0$, while $\nu = 1.0$ ($t' = t'' = t_0/\sqrt{2}$), the pure 2LSU2 state, implies $\phi = \pi/4$. In what follows we will assume, for simplicity, that $U = U'$.[21]

Figure 1(a) shows a schematic representation of $H_{\rm tot}$, together with diagrams indicating the gradual decoupling of bands from the QD [Figs. 1(b) and 1(c)] as the symmetries of the system are exploited, finalizing with the construction of the MOs $|+\rangle$ and $|-\rangle$. A brief description of these transformations is given below and full details are provided in Appendix A.

B. Molecular orbitals: band decoupling

Given the left-right symmetry of the system, two bands decouple from the QDs, as indicated in Fig. 1(b), through a symmetric-antisymmetric combination of creation-annihilation operators from left and right leads (without mixing α and β states). The resulting system [see Fig. 1(b)] still has one more symmetry to be exploited. If one performs a symmetric-antisymmetric linear

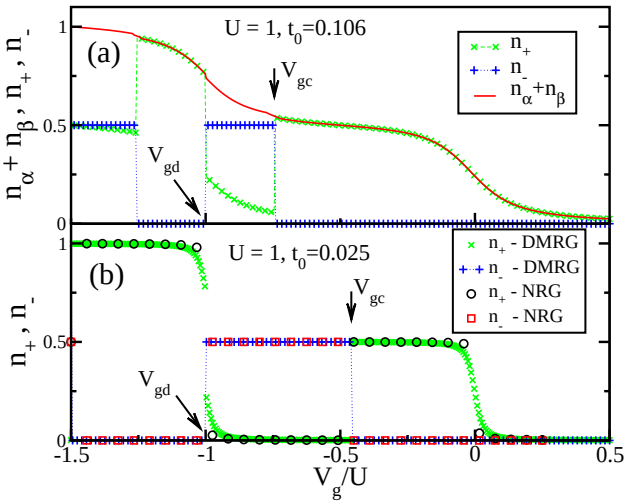

FIG. 2: (Color online) (a) DMRG results for charge variation against gate potential: $n_+(V_g)$, (green) $\times$ symbols, $n_-(V_g)$, (blue) $+$ symbols, and $n_\alpha + n_\beta$, (red) solid line (note that $n_\alpha = n_\beta$). The charging of the AOs is smooth, while the charging of the MOs has clear discontinuities. The parameters used are $\phi = \pi/4$, $t_0 = 0.106$ ($\Gamma = 0.045$), $U = 1$, and $\Gamma = 0.045$ (note that the particle-hole symmetric point of this model is at $V_g = -3U/2$, and the charge is plotted *per spin species*). (b) Comparison between NRG and DMRG $n_\pm$ *vs.* V_g results for the 2LSU2 state ($\phi = \pi/4$, $t_0 = 0.025$ ($\Gamma = 0.0025$), and $U = 1$). NRG: n_+ [circles (black)], n_- [squares (red)]. DMRG: n_+ [$\times$ (green)], n_- [$+$ (blue)]. Note the very good agreement between the two techniques. DMRG results obtained with 40 sites and maintaining 200 states. NRG results obtained at the last iteration (N=80), and a discretization parameter $\Lambda = 2.5$ was used, keeping $N_s = 1500$ states in each iteration, which allows a larger N_s to account for degeneracies (all the other NRG calculations in this work were done similarly). The small differences occur because the DMRG results are not totally converged yet. Note also [as in panel (a)] the interesting V_g-dependent charge oscillations involving the two MOs simultaneously, given that they are capacitively coupled. See text for definition of V_{gc} and V_{gd}.

combination of α^{even} and β^{even} creation-annihilation operators acting on sites situated at the same distance from the QD [see Fig. 1(b)] *and* a bonding-antibonding linear combination of the QD levels $|\alpha\rangle$ and $|\beta\rangle$, one obtains the MOs $|+\rangle$ and $|-\rangle$, which couple to symmetric and antisymmetric bands, respectively, as shown in Fig. 1(c), through hopping matrix elements

$$t_+ = \sqrt{2}(t' + t'') \tag{5}$$

$$t_- = \sqrt{2}(t' - t'') \tag{6}$$

It is now clear that, *at* the 2LSU2 point (where $\nu = 1$, i.e., $t' = t''$, and therefore $t_- = 0$), a third band decouples from the system, leaving MO $|-\rangle$ decoupled from any electron reservoir, although still capacitively coupled to MO $|+\rangle$. This immediately answers some of the questions raised above. First, in the limit $\nu \to 1$, the charge transport changes from double- to single-channel. Therefore, the maximum conductance will change from $2G_0$ to G_0. Indeed, in the vicinity of the 2LSU2 point, for $\nu \lesssim 1.0$, narrow peaks with height $2G_0$ are expected around certain values of gate potential. The closer one gets to the 2LSU2 point, the narrower these peaks become, their width vanishing at the 2LSU2 point, where the maximum of the conductance will be G_0.[10,17] Second, at the 2LSU2 state, MO $|-\rangle$, being decoupled from the charge reservoir, will have zero width, i.e., Γ_- vanishes (for a definition of Γ_-, see below and Appendix A). As the gate potential varies, and after the level $|-\rangle$ has crossed the Fermi energy, it will be abruptly charged, changing the ground state of the system (recall that MO $|-\rangle$ has a many-body interaction with the rest of the system), and potentially changing its transport properties discontinuously. One should expect that the Kondo peak in the LDOS, when the system is in the SU(4) state, should differ considerably from the Kondo peak occurring in the 2LSU2 state, given the difference in the number of charge transport channels between the two states. The very abrupt change in the slave boson's LDOS (seen in Fig. 14 of reference 9) is probably linked to this change from double- to single-channel charge transport. If the change in the Kondo resonance is discontinuous or not (at $\phi = \pi/4$) is still a point to be further investigated.

For completeness, we present here $H_{\rm mb}$ written in the new basis, assuming that $U = U'$ (in Appendix A, a complete expression, for the case $U \neq U'$ is presented)[31],

$$H_{\rm mb} = \frac{U + U'}{4}\left[\sum_{\lambda,\sigma} n_{\lambda\sigma} n_{\lambda\bar{\sigma}} + \sum_{\lambda\neq\lambda',\sigma} n_{\lambda\sigma} n_{\lambda'\bar{\sigma}}\right] +$$

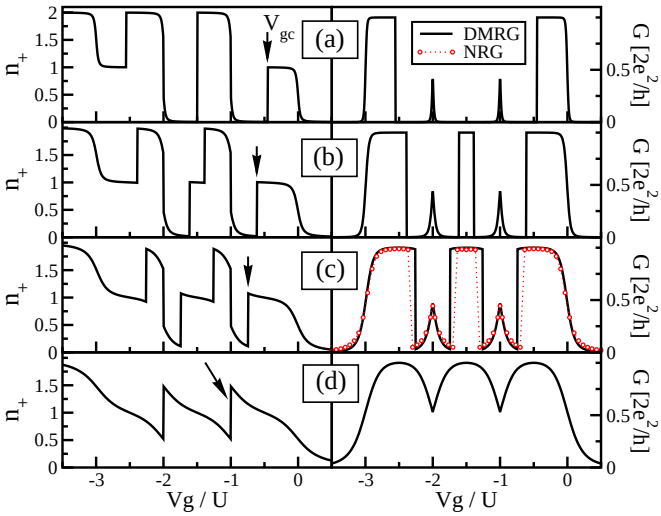

FIG. 3: (Color online) Left panels: DMRG results similar to the ones in Fig. 2, but now for varying t_0 (0.025, 0.05, 0.106, and 0.175, from top to bottom). The corresponding values for Γ are 0.0025, 0.01, 0.045, and 0.1225. $U = 1.0$ for all panels. For the sake of clarity of presentation, just the n_+ results are shown. Note that the value of V_{gc} [gate potential for charging (discharging) of $|-\rangle$ ($|+\rangle$)] is strongly dependent on Γ, while V_{gd} (gate potential for discharging (recharging) of $|-\rangle$ ($|+\rangle$)] is not (its value is practically fixed at $V_g/U = -1.0$). Right panels: Solid (black) lines: conductance obtained through the Friedel sum rule applied to the corresponding charges in the left panels. (Red) Dots in panel (c): NRG results for the conductance. Notice the good agreement between the two techniques. The narrow peaks in the 3 top right panels, located at $V_g/U = -1.0$, are briefly discussed in the text. OBS.: The bottom right panel should be compared to Fig. 4 in Ref. 10. The fact that only one NRG result is shown in the right-side panels is explained in the text.

$$\frac{U'}{2} \sum_{\lambda \neq \lambda', \sigma} n_{\lambda\sigma} n_{\lambda'\sigma} \tag{7}$$

where $\lambda = \pm$, $\sigma = \uparrow$ or $\downarrow$, and although our calculations are for $U = U'$, both are indicated, with their respective terms. It is also useful to define the broadening of the one-body AOs $|\alpha, \beta\rangle$, as well as for the MOs $|\pm\rangle$ (coming from their coupling to the leads). For the AOs, we have

$$\Gamma = \Gamma_\alpha + \Gamma_\beta, \tag{8}$$

$$\Gamma_{\alpha/\beta} = 2\pi(t'^2 + t''^2)\rho_0(E_F) = 2\pi t_0^2 \rho_0(E_F), \tag{9}$$

where the factor 2 in Eq. 9 takes in account the left *and* right leads [see Fig.1 (a)], and $\rho_0(E_F)$ is the LDOS at the first site of the leads (here considered the same for the α and β channels), and Γ is the total coupling between the interacting region and the leads. For the MOs we have

$$\Gamma_+ = \pi t_+^2 \rho_0(E_F), \tag{10}$$

$$\Gamma_- = \pi t_-^2 \rho_0(E_F). \tag{11}$$

Note that, as required, $\Gamma = \Gamma_+ + \Gamma_-$ (for more details, see Appendix A).

The MO $|-\rangle$, in the 2LSU2 regime ($\nu = 1$), is an electronic *dark state* that cannot interact directly with the conduction electrons. Such state has been extensively studied in different systems, namely, as Dicke effect[22–24] or bound states in the continuum (BICs),[25,26] which can produce Fano resonances in the conductance.[27] The original Dicke effect in quantum optics[28] takes place through spontaneous emission, by two closely spaced atoms (of the same species), which emit a photon into a common environment.

III. CHARGE OSCILLATION OF MOLECULAR ORBITALS: DMRG AND NRG RESULTS

A. DMRG and NRG (zero and finite-temperature) results

In this section, we describe the 2LSU2 gate-potential-dependent charge oscillations associated to the presence of the dark state. In section III.B, we show that the effect of the charging of the dark state $|-\rangle$ over the MO state $|+\rangle$ can be incorporated

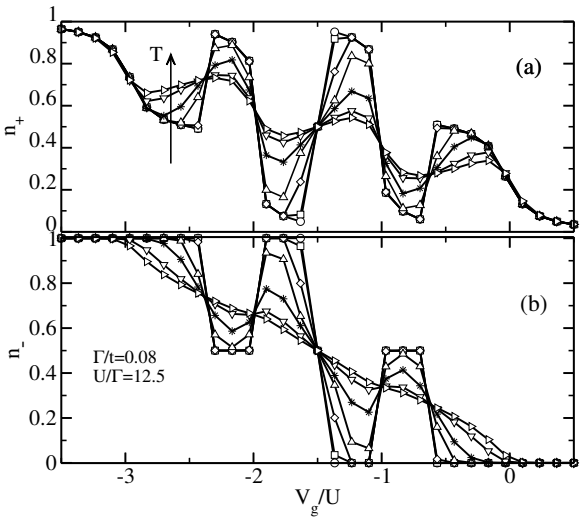

FIG. 4: Temperature (in units of U) dependent NRG results for $n_\pm$ $vs.$ V_g. Maximum temperature (right pointing triangles) is $T = 3.118 \times 10^{-2}$ [minimum temperature is zero (circles)]. The arrow in panel (a) indicates direction of temperature increase. Note that the MO V_g-dependent charge oscillations have been strongly suppressed at $T = 7.888 \times 10^{-3}$ (stars), a value that is of the same order of magnitude as the Kondo temperature of a corresponding (same parameters) single impurity problem. This suggests that the MO charge oscillations arise from a low-energy effect, possibly related to the Kondo effect. Parameters are indicated in the bottom panel.

into an effective gate potential acting over MO $|+\rangle$. This is based on the fact that (in the 2LSU2 state) the MO $|-\rangle$ can only contain an integer number of electrons. The definition of this effective gate potential greatly helps the understanding of the gate-potential-dependent charge oscillations.

Figure 2(a) contrasts DMRG results at the 2LSU2 state ($\phi = \pi/4$) obtained for $n_\pm$ $vs.$ V_g and $n_{\alpha,\beta}$ $vs.$ V_g, emphasizing the difference between them: the AOs present a smooth charging, as a function of V_g, and, obviously, $n_\alpha(V_g) = n_\beta(V_g)$, while $n_\pm(V_g)$ show clear discontinuities and very diverse behavior. Note that we plot only up to the p-h symmetric point ($V_g/U = -1.5$), and the data has to be multiplied by 2 to reproduce the total charge in the QD, i.e., we are plotting charge per spin species, as the system is SU(2) invariant. Figure 2(b) shows a comparison of $n_\pm$ $vs.$ V_g between NRG and DMRG, at zero-temperature. The agreement between the two techniques is quite good, as can be easily seen. The hopping and many-body parameters used are indicated in the figure and in the caption, and $\phi = \pi/4$ for both panels (2LSU2 *state*). As mentioned above, at the 2LSU2 state, level $|-\rangle$ is completely decoupled from the electron reservoir and will obviously be abruptly charged for some V_g value, and, given that it is capacitively coupled to level $|+\rangle$, its occupancy will also change abruptly. This is clearly reflected in the results for $n_\pm$ in Figs. 2(a) and (b). Note that the results in Fig. 2(a) are for a smaller value of U/Γ than those in Fig. 2(b) (the second is deeper into the Kondo regime), although this discontinuity in the charge occupancy of the MOs still occurs for both cases. Note that the log-discretization of the semi-infinite chain used by NRG is the one described in Ref. 29.

The questions to be answered here are the following: (i) what determines the value of V_g for which the charging (discharging) and discharging (recharging) of level $|-\rangle$ ($|+\rangle$) occurs (indicated in Fig. 2(a) with arrows and denoted V_{gc} and V_{gd})? (ii) How this value depends on Γ? (iii) And finally, how robust is this phenomenon? I.e., how far from the *strict* 2LSU2 regime can we go (i.e., for $\phi < \pi/4$) and still observe this gate potential dependent MO charge oscillation effect? Why this charge oscillation effect is important will be apparent soon (see Fig. 6).

Figure 3, showing DMRG results for different values of U/Γ, answers the second question. I.e., how does the charging of MO level $|-\rangle$ depends on Γ (for fixed U)? In it, on the left side panels, one sees that V_{gc} depends on Γ much more strongly than V_{gd}, as the value of V_{gd} barely changes with Γ, while V_{gc} decreases as Γ increases, until $V_{gc} = V_{gd}$ (a full explanation of this effect will be given in section V). To underscore the fact that for $\phi = \pi/4$ charge transport occurs *only* through MO $|+\rangle$, the right panels in Fig. 3 show the conductance results obtained by using the Friedel sum rule (solid curves) $G = G_0 \sin^2(\pi n_+/2)$, where the results used for $n_+(V_g)$ are those obtained by DMRG (left panels). The dotted curve in panel (c) shows the conductance results obtained by NRG (through the calculation of the dressed Green's function). The good agreement between both techniques indicates that, as expected, the conductance is all through the molecular orbital $|+\rangle$. The origin of the sharp peak at $V_g/U = -1.0$ will be explained in section IV, where the LDECA results for conductance are presented. Note that the lack of NRG results for the other right-side panels is due to convergence issues.[30]

To help answer the other questions, it is important to have an idea of the order of magnitude of the energy scale of the processes that determine this gate potential dependent charge oscillation. The temperature (in units of U) dependent $n_\pm$ $vs.$ V_g NRG results in Fig. 4 indicate that these V_g-dependent charge oscillations have been strongly suppressed at a temperature which is a very small fraction of U (see temperature values in the caption). Indeed, as the charge transport occurs through level $|+\rangle$,

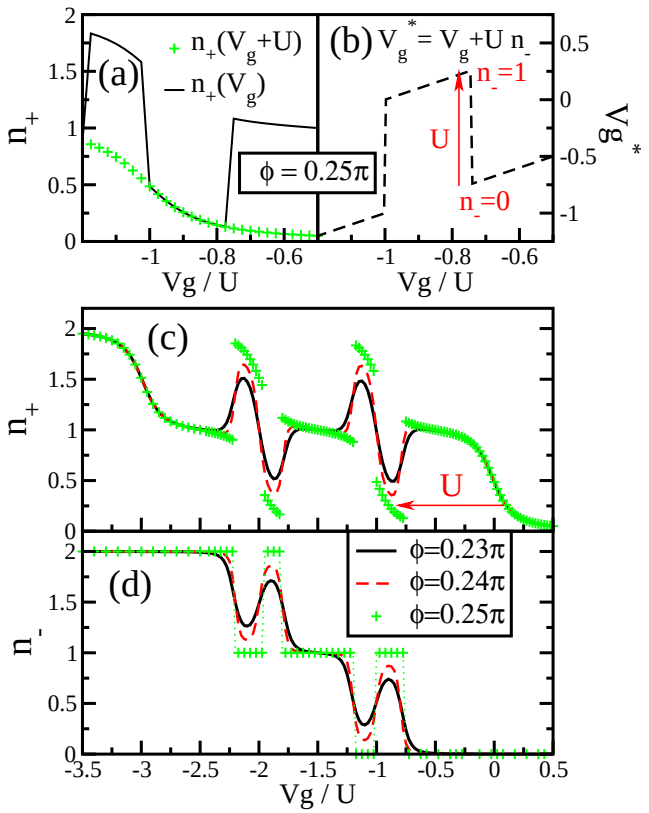

FIG. 5: (Color online) (a) n_+ *vs.* V_g DMRG results ($U = 1.0$, $\Gamma = 0.045$, and $\phi = \pi/4$) comparing $n_+(V_g)$, solid black line, with $n_+(V_g + U)$ [(green) + symbols] for V_g values around $-0.9U$. The perfect agreement between the two curves, in the region between discontinuities, indicates the simple fact that the charging of the decoupled MO level $|-\rangle$ acts as an extra electrostatic potential, moving up by U the effective potential seen by MO level $|+\rangle$. This is schematically shown in (b), where the effective potential is plotted against V_g and the (red) vertical arrow indicates the charging of MO $|-\rangle$ and the change by U of the effective potential seen by MO $|+\rangle$ (the discharging of MO $|-\rangle$ occurs in the other discontinuity). (c) and (d): DMRG results for $n_\pm$ *vs.* V_g for three different values of ϕ/π (0.25, 0.24, and 0.23). This shows that the V_g-dependent charge oscillations seen *at* $\phi/\pi = 0.25$ survive away from the 2LSU2 point. The charge oscillations are still noticeable down to $\phi/\pi \approx 0.2$ (not shown). The parameters are $t_0 = 0.106$, $\Gamma = 0.045$, and $U = 1.0$. The DMRG calculation was done for a cluster with 80 sites and 200 states were kept, and for $\phi < 0.25$ only the left-right transformation was used [see Fig. 1(b)] The (red) horizontal arrow in panel (c), when applied to the (green) + symbols curve, schematically shows the displacement presented in panel (a).

as shown by the description of the DMRG results presented in Fig. 3, the Kondo temperature of the system is in reality that of a single QD with the same Γ and U as that of level $|+\rangle$. This Kondo temperature, calculated using NRG, is of the same order of magnitude as the temperature for which the V_g-dependent charge oscillations have been strongly suppressed ($T \approx 7.888 \times 10^{-3}$, $*$ curve). This indicates that, as initially thought, these charge oscillations are governed by a many-body process related to the Kondo effect, or some other many-body effect with a similar characteristic energy (as shown in Appendix B, the non-interacting model, $U' = U = 0$, does not show these V_g-dependent charge oscillations).

B. The effective gate potential model ($\phi = \pi/4$)

From the point of view of level $|+\rangle$, level $|-\rangle$, when charged, acts as an extra source of electrostatic energy, besides the one provided by the back-gate (V_g). The particularities here are that, *at* the 2LSU2 point ($\phi = \pi/4$), level $|-\rangle$, being decoupled from the electron reservoir, can only accommodate an integer number of electrons ($n_- = 0$, 1, or 2). Taking this into account, one can define an effective gate potential as $V_g^* = V_g + Un_-$. From this point of view, it is then easy to understand the effect of the charging and discharging of level $|-\rangle$: it just modifies the *effective* gate potential seen by level $|+\rangle$. To emphasize that this is indeed the only effect in play for the charging of level $|+\rangle$ at the 2LSU2 state, we show in Fig. 5(a) the curves for $n_+(V_g)$ and $n_+(V_g + U)$ for V_g/U values around -0.9 [for $U/\Gamma = 22.0$, corresponding to Fig. 3(c)]. The horizontal arrow in Fig. 5(c)

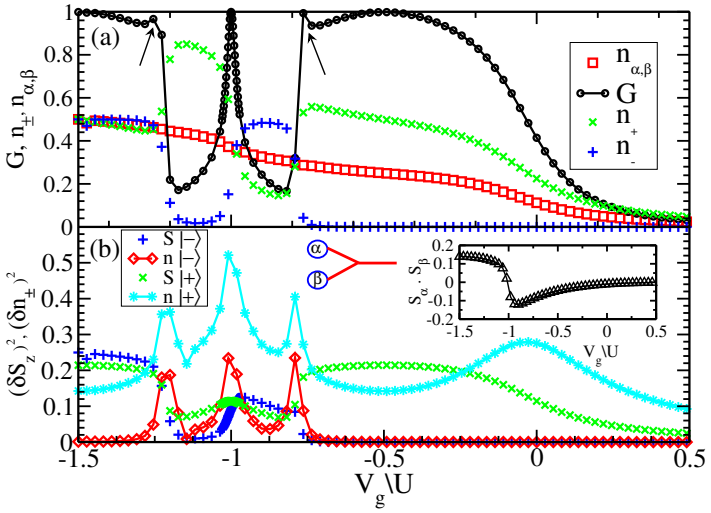

FIG. 6: (Color online) (a) LDECA results ($t_0 = 0.15$, $\Gamma = 0.09$, $U = 1.0$, $\lambda = 7$, and $\phi = 0.242$) for conductance G [(black) circles], charging of the MO levels $n_\pm$ ($\times$ (green) and $+$ (blue) symbols for n_+ and n_-, respectively), and charging of the AO levels $n_{\alpha,\beta}$ (square (red) symbols). The mere comparison of G with $n_\pm$ and with $n_{\alpha,\beta}$ indicates that the conductance variation with V_g is intimately correlated with that of $n_\pm$, i.e., understanding the V_g-dependent charge oscillations of the MOs $|\pm\rangle$ is crucial to the understanding of the charge transport properties of the system. In addition, by comparison with Figs. 5(c) and (d), one notices the qualitative agreement between the DMRG and LDECA results for $n_\pm$ as a function of V_g. (b) LDECA results for spin and charge fluctuations for both MOs. $\times$ symbols (green) and $+$ symbols (blue) indicate $(\delta S_z)^2$ for MO $|+\rangle$ and $|-\rangle$, respectively; diamonds (red) and $*$ (cyan) indicate $(\delta n)^2$ for MO $|-\rangle$ and $|+\rangle$, respectively. A plateau in $(\delta S_z)^2$, accompanied by simultaneous suppression of charge fluctuations, indicates a level participating in a Kondo effect. It is interesting to note that, according to these results, MO level $|-\rangle$, although very weakly coupled to the charge reservoir, and therefore still undergoing strong V_g-dependent charge oscillations (notice that $\phi \sim \pi/4$), seems to participate in the Kondo effect, mainly close to the p-h symmetric point, where its spin fluctuations are higher than those for MO $|+\rangle$. The inset shows the results for spin-spin correlations between the AO levels $|\alpha\rangle$ and $|\beta\rangle$ (vertical triangles). Note that close to the p-h symmetric point they are ferromagnetically correlated. The cartoon at the left side of the inset explains why (see text and Reference 35). The conductance structures indicated by small arrows in panel (a) are discussed in the text. Note that the charge fluctuation for MO $|+\rangle$ [$*$ (cyan)] was divided by 2 to fit better in panel (b).

schematically shows the 'superposition' of the two curves shown in Fig. 5(a). The matching of the two curves in Fig. 5(a), for $n_+(V_g)$ [solid (black)] and $n_+(V_g + U)$ [(green) $+$ symbols], in the region between discontinuities, is perfect, confirming the effective potential idea described above: the discontinuous charging of the MO $|-\rangle$ changes by U the gate potential seen by MO $|+\rangle$, discharging it by 1 electron (as the total charge in the system is kept constant), and, more importantly, as V_g decreases further below V_{gc}, the *recharging* of MO $|+\rangle$ occurs exactly the same way [see Fig. 5(a)] as when MO $|-\rangle$ was empty, at $V_g = V_{gc} + U$. As a reference, the effective gate potential V_g^*, as a function of V_g, is shown in Fig. 5(b). The question still to be answered is what physical process determines $V_{gc}(\Gamma)$, i.e., the dependence of the value of V_{gc} with the coupling to the leads Γ (as depicted in the left-side panels of Fig. 3). Before answering this question, let us concentrate on the other two pending issues: how robust is this gate-dependent charge oscillation away from the exact 2LSU2 point, and what is its effect over the charge transport, i.e., the conductance of the system.

IV. DMRG AND LDECA RESULTS AWAY FROM THE 2LSU2 POINT

Figures 5(c) and (d) show DMRG $n_\pm$ *vs.* V_g results for three different values of ϕ/π (0.25, 0.24, and 0.23). As expected, the discontinuities are smoothened out, but the charge oscillations survive. Additional calculations (not shown) indicate that the oscillations are still noticeable for $\phi/\pi \approx 0.2$ ($t''/t' \approx 0.73$). Once $\phi < \pi/4$, the transport problem becomes a double channel one, making its solution through NRG much more costly in computational terms. To circumvent this, here we use the LDECA method[16] to present results for $\phi < \pi/4$. Fig. 6(a) shows results for conductance G (* (black) symbols), and $n_\pm$ *vs.* V_g for $\phi/\pi = 0.242$ ($\times$ (green) and $+$ (blue) symbols for n_+ and n_-, respectively). The (red) square symbols show the charging of the AO levels $|\alpha,\ \beta\rangle$. A comparison of the conductance curve with the curves for the charging of the MO levels and the AO levels indicates that the charging of the AO levels provides very little information about the sharp features observed in the conductance. These features are obviously more correlated to the charging of the MOs. As $\phi \approx \pi/4$, we are still too close to the single-channel regime, and the conductance is still too close to those obtained in Fig. 3 (right-side panels). The charging results for the MO levels are in good qualitative (and even quantitative) agreement with those for DMRG [as shown in Figs. 5(c) and (d)].

It is interesting to contrast the very sharp peak in the conductance, around the point where level $|-\rangle$ is discharged, with the ones shown in the right-side panels in Fig. 3. In Fig. 5(a), the peak reaches one quantum of conductance (G_0), while in Fig. 3 it reaches just $\approx G_0/2$). Although the convergence of LDECA results as $\phi \to \pi/4$ becomes increasingly difficult, the peak at $V_g = -U$, for $\phi < \pi/4$, has always a maximum of G_0. We speculate that the difference with the $\phi = \pi/4$ results (Fig. 3) stems from the number of channels. Although Γ_- is very small when $\phi \approx \pi/4$, there *are* two channels available for charge transport (contrary to the situation at $\phi = \pi/4$). Notice in Fig.5(a) that the discharging of MO $|-\rangle$ (at $V_g/U \approx -1$) occurs over a window of V_g (with width Γ_-), indicating that level $|-\rangle$ is in resonance with the band, therefore participating in charge transport. LDECA results for smaller values of ϕ (down to $\phi/\pi \sim 0.2$) indicate a smooth evolution of the conductance, until values of G start to show features above G_0, once the double channel transport takes hold (and the conductance reaches $2G_0$ for some narrow regions of V_g).[32]. In addition, a comparison of the right side tail of the narrow peak, with the corresponding right tail of the broad plateau (approximately centered around $V_g/U = -U/2$) shows that the effective potential idea is still helpful in interpreting the results (at least for this small deviation from $\phi = \pi/4$). Note that n_- (+ (blue) symbols) is still very approximately quantized. Finally, it is interesting to point out that the small upticks in the conductance, before the sharp drop, and after the sharp rise (indicated with arrows) have been seen in functional Renormalization Group (fRG) calculations, for a similar model, by C. Karrasch *et al.* [see their Fig. 5(a)].[33]

In Fig. 6(b), results for spin and charge fluctuations for the MOs are shown. As expected, the rightmost conductance plateau in panel (a) is associated to a plateau in the spin fluctuations of MO level $|+\rangle$ ($\times$ (green) symbols), and a suppression of its charge fluctuations (* (cyan) symbols), which are fingerprints of the Kondo effect. Taking in account the comment above, that the effective gate potential model is still useful, the narrow peak around $V_g/U = -1.0$ can then be interpreted as a Kondo state that was 'skipped' due to the second charge oscillation: indeed, when MO $|-\rangle$ discharges approximately 1 electron, the effective potential seen by MO $|+\rangle$ abruptly decreases by $\sim U$, moving the system from the high V_g side of the Intermediate Valence regime to its low V_g side, completely skipping the Kondo regime (note the enhancement of charge fluctuations for MO $|+\rangle$ around $V_g/U = -1.0$, and a much smaller value for its spin fluctuations, as compared to the right-side maximum, indicating that the charge transport process here is more akin to sequential tunneling)[34]

Around the p-h symmetric point, a Kondo effect with peculiar characteristics arises, where *both* MOs participate. This can be confirmed by checking the spin fluctuations of MOs $|+\rangle$ *and* $|-\rangle$. In reality, the spin fluctuations of MO $|-\rangle$ (+ (blue) symbols) are (surprisingly!) more enhanced than those of MO $|+\rangle$. Given the capacitive coupling between the two MOs, the participation of level $|+\rangle$ in a Kondo effect drives level $|-\rangle$ into also becoming an active degree of freedom in the Kondo effect. A somewhat different view of this Kondo effect can be taken if one returns to the AO basis and calculates the spin correlations between AOs $|\alpha\rangle$ and $|\beta\rangle$. This is shown in the inset in Fig. 6(b): the two AO states, close to the p-h symmetric point develop a *ferromagnetic* correlation. This can be readily understood by referring to Fig. 1(b): instead of performing the symmetric/antisymmetric *and* the bonding/anti-bonding transformations that lead to Fig. 1(c), one should skip the second transformation (keeping the AOs). This leads to (for $\nu = 1$) the schematics shown at the left side of the inset in Fig. 6(b), which is well known to lead to ferromagnetic correlations between the AOs, as remarked by Martins *et al.*[35] and confirmed in other publications thereafter.[36]

V. COMPETITION BETWEEN KONDO AND INTERMEDIATE VALENCE EFFECTS ($\phi = \pi/4$)

The origin of the dependence of V_{gc} with the coupling to the leads (Γ), as shown in the left panels of Fig. 3, still has to be understood. In Fig. 4 we have shown that the V_g-dependent charge oscillations are related to a low energy scale phenomenon. Another important point that has to be remarked, is that the very dependence of V_{gc} with Γ clearly indicates that the MO level $|-\rangle$ does not get charged the moment it crosses the Fermi energy, as V_g varies. This conclusion is obvious from the fact that the position of the Fermi energy is the same for all left-side panels in Fig. 3, and still, the level $|-\rangle$ gets charged at different gate potential values. This is a consequence of MO level $|-\rangle$ being strongly correlated to the whole system, including the electron reservoir, through MO $|+\rangle$. Bearing in mind now that the charging of level $|-\rangle$ *at a certain* V_g *value* results in 'moving back' level $|+\rangle$ from a Kondo state to an Intermediate Valence state by increasing its effective gate potential by U, one may assume that it is energetically more favorable for the system *at that* V_g *value* to have MO level $|+\rangle$ in the Intermediate Valence state than in the Kondo state. By using DMRG to calculate the ground state energy of a *Single Impurity Anderson Model* (SIAM) as a function of V_g, this intuitive idea can be quantitatively probed. To achieve that, one just has to remove from the SIAM ground state energy, calculated with DMRG, its single-electron contributions, i.e., $H_{\rm band}$, the gate potential energy, and the *local* correlation energy $U\,(n_\downarrow\, n_\uparrow)$, thus defining the following energy, here denoted as $T_0\,(V_g)$:

$$T_0(V_g) = E_0(\Gamma = 0, V_g) - E_0(\Gamma, V_g), \tag{12}$$

where $E_0(\Gamma, V_g)$ indicates the ground state energy (calculated with DMRG) for a SIAM with parameters $U = 1$, and hopping to the band equal to $t_+ = 2t_0$ [for $t_0 = 0.025$, corresponding to Fig. 3(a)], while $E_0(\Gamma = 0, V_g)$ is the corresponding ground state energy for the same model and same parameters, but now with the impurity disconnected from the band. Note that, as $T_0\,(V_g) > 0$, it represents the gain in energy, by the system, when the many-body correlations are extended into the leads (be it

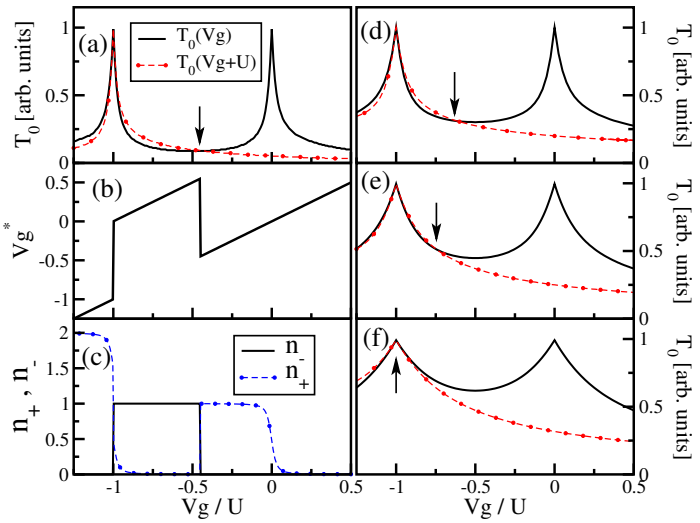

FIG. 7: (Color online) (a) Comparison of $T_0(V_g)$ (solid (black) curve) with $T_0(V_g+U)$ (dotted (red) curve) for a large window of V_g. Notice the crossing point for the two curves (indicated by an arrow). As can clearly be seen, this is the point for which the gain in energy (T_0) by 'moving up' the effective gate potential of the system by U, and going back to the Intermediate Valence regime, is larger than the gain in energy provided by 'staying' in the Kondo state. It can be clearly seen in panels (b) and (c), which show the effective gate potential and corresponding results for $n_\pm(V_g)$, respectively, that the crossing indicated in panel (a) exactly agrees with V_{gc}, i.e., the point where n_- is charged and n_+ is discharged. In addition, the second charge oscillation (at $V_{gd}/U=-1$) occurs at the point where $T_0(V_g+U)$ crosses $T_0(V_g)$ for the second time, but now passing *under it*. In this case, it is energetically favorable for the system to 'move down' the effective potential, i.e., when the system starts to enter the Kondo regime again, it is energetically advantageous for the system to 'skip' the whole Kondo regime and go straight to the second Intermediate Valence regime. This is accomplished by MO level $|-\rangle$ being discharged and level $|+\rangle$ being recharged. Parameters used in panels (a) to (c) are the same as the ones used in Fig. 3(a). Panels (d) to (f) show similar results as in panel (a), but for progressively larger values of Γ (the same parameters as the ones used in panels (b) to (d) in Fig. 3). For all the cases analyzed, the crossing of $T_0(V_g)$ and $T_0(V_g+U)$ agrees with V_{gc}.

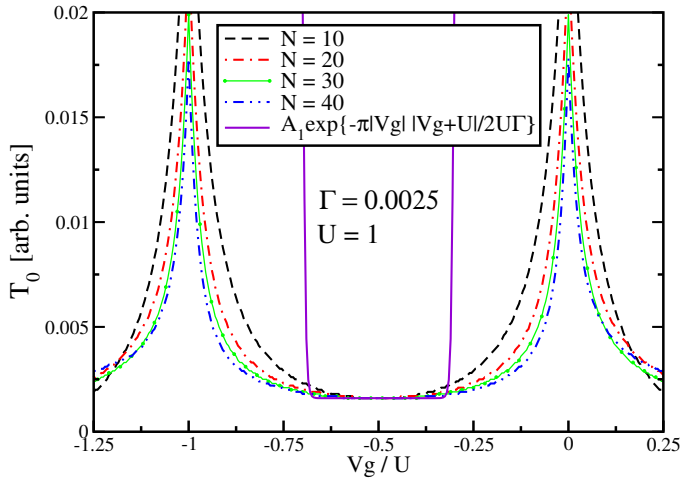

FIG. 8: (Color online) Comparison of the DMRG finite size scaling calculation of T_0 (see text for its definition), with the Haldane expression for T_K, Eq. (13). Curves for $N=10$, 20, and 30, were translated to match the $N=40$ curve at $V_g/U=-0.5$. The same translation was applied to Haldane's curve. It is clear that, in the region of V_g where the Haldane expression applies (before it diverges), the DMRG results for larger clusters gradually approach Haldane's results. Parameters are the same as the ones used in Fig. 3(a).

by the formation of the Kondo state, or any other strongly correlated ground state).[37] We find out, as shown in Fig. 7, that this energy $T_0\,(V_g)$ explains the dependence of V_{gc} with Γ.

In Fig. 7(a), the energy T_0 is plotted as a function of V_g, and, as done in Fig. 5(a), we compare $T_0(V_g)$ (solid (black) curve) with $T_0(V_g+U)$ (dot-dashed (red) curve). The 'horizontal displacement' of T_0 by U (dot-dashed (red) curve) mimics the effect over MO $|+\rangle$ (the *single impurity* in the SIAM) of the charging of MO $|-\rangle$. The arrow in Fig.7(a) indicates the crossing point of the two curves, i.e., the point for which the *gain in many-body energy* T_0, by 'moving up' the gate potential of the system

by U, and going back to the Intermediate Valence regime (dot-dashed (red) curve), is larger than the gain in energy provided by 'staying' in the Kondo state [(black) solid curve]. What affords the double-MO system (with MO levels $|+\rangle$ and $|-\rangle$) the ability to put in direct competition two states relatively distant in the phase diagram (the center of the CB valley and the initial ramp up of the CB peak) is the presence of the zero-width strongly correlated MO level $|-\rangle$ that can be charged abruptly and can only contain an integer number of electrons (for $\phi = \pi/4$, or approximately integer for $\phi \lesssim \pi/4$). Panels (b) and (c) in Fig. 7 show the effective gate potential (as a function of V_g) and the corresponding results for $n_{\pm}(V_g)$, respectively, for the same parameters used to calculate T_0 ($U = 1.0$, $t_0 = 0.025$) for the SIAM in panel (a), but for the model containing both MO states. The crossing indicated in panel (a) (vertical arrow) agrees *exactly* with V_{gc}, i.e., the point where n_- is charged and n_+ is discharged. In addition, the second charge oscillation (at $V_{gd}/U = -1$) occurs at the point where $T_0(V_g + U)$ crosses $T_0(V_g)$ for the second time, i.e., when MO level $|+\rangle$ starts to enter the Kondo effect again (dot-dashed (red) curve in panel (a), around $v_g/U = -1$), it is energetically advantageous for it to 'move down' (by decreasing the effective potential by U, as n_- changes from 1 to 0), thus 'skipping' the whole Kondo regime and going straight to the second Intermediate Valence regime. This is accomplished by MO level $|-\rangle$ being discharged and level $|+\rangle$ being recharged (and this 'skipping' of the Kondo regime results in the narrow peak seen in the conductance in Fig. 5(a), centered around $V_g/U = -1.0$). Panels (d) to (f) show similar results as in panel (a), but for progressively larger values of Γ (the same parameters as the ones used in panels (b) to (d) in Fig. 3). For all the cases analyzed, the first crossing of $T_0(V_g)$ and $T_0(V_g + U)$ agrees with V_{gc}, and, as can be clearly seen, the second crossing occurs always at the same gate potential $V_g/U = -1.0$ [note that in panel (f), the two crossings now coincide, resulting in the peculiar charging pattern in Fig. 3(d)].

As initially hinted by the finite temperature NRG results in Fig. 4, the gate potential dependent charge oscillation effect is a low-energy many-body effect; in reality, an interesting competition between two different many-body states, Kondo and Intermediate Valence. The ability of the DMRG calculated $T_0(V_g)$ to explain this subtle effect motivates us to compare T_0 with the well known Haldane expression for T_K,[20,38]

$$k_B T_K \sim D \left(\frac{\Gamma U}{|V_g||V_g + U|} \right)^{1/2} e^{-\pi |V_g||V_g+U|/2\Gamma U} . \tag{13}$$

Fig. 8 does just that for a system consisting of a *single* QD. A finite size scaling of T_0, for DMRG clusters of increasing size, $N = 10$, 20, 30, and 40 (where N is the total number of sites in a DMRG one-dimensional cluster containing the impurity plus $N - 1$ non-interacting sites), shows that T_0, in the V_g region around the p-h symmetric point, where the Haldane expression applies, is tending to Haldane's T_K. The parameter values are indicated in the figure. A few points have to be stressed here. First, note that the objective of Fig. 8 was not to attempt a simulation of the absolute value of T_K (all the curves have been translated in energy so that they coincide with the $N = 40$ value at the p-h point). The objective at this point is to reproduce the dependence of T_K with gate potential V_g. Second, note that the Haldane expression is by no means exact, and is supposed to be applicable only when real charge fluctuations of the impurity can be neglected, therefore we are not expecting a complete agreement of DMRG results with Haldane's T_K. With these two points in mind, and taking into account that a larger DMRG computational effort (not attempted in this work) can greatly improve the accuracy of the T_0 results, one can, after a careful analysis of different definitions for T_0, propose a DMRG calculation of T_0 as a useful guide to experimentalists for all the relevant regimes of the single impurity Anderson model.[39]

VI. CONCLUSIONS

In this work, motivated by recent interest in CNT QD charge transport measurements, the authors use three distinct numerical techniques to study the 2LSU2 regime and present details of its properties, which hinge in two important aspects: first, a transformation from atomic to molecular orbitals is needed to understand the numerical results for charge transport. Second, this transformation unveils an interesting gate-potential-dependent charge oscillation involving two strongly interacting molecular orbitals, one of which, MO $|+\rangle$, is coupled to the band, while the other, MO $|-\rangle$, is totally decoupled from it (*at* the 2LSU2 state), while capacitively coupled to $|+\rangle$. In doing that, a series of unanswered questions associated to the 2LSU2 regime are clarified. First among them is the fact that *at* the 2LSU2 regime the maximum conductance passes from $2G_0$ to G_0, as the charge transport changes from double- to single-channel. In addition, all the charge transport properties specifically associated to the 2LSU2 state are shown to be robust, in the sense that they can in principle be observed even when there is no total mixing of the orbital quantum numbers ($\phi < \pi/4$). Finally, by numerically defining the quantity T_0, it is shown that this gate dependent charge oscillation results from the competition between the Kondo and Intermediate Valence states. These two states, separated by a wide crossover region, can be effectively put in contact by the presence of a strongly correlated *dark state* (i.e., a zero width state), the MO $|-\rangle$. By comparing our numerical results for T_0 with Haldane's T_K, we speculate that the DMRG results obtained by this relatively easy computational calculation may be of interest to experimentalists in the analysis of other systems. A more refined analysis of T_0 is now being pursued and will be presented elsewhere. In addition, it will be the subject of a forthcoming work to understand how the phenomena observed in the 2LSU2 regime change for $U' \neq U$ and when the degeneracy of the AOs $|\alpha\rangle$ and $|\beta\rangle$ is lifted.

Acknowledgments

It is a pleasure to acknowledge useful conversations with K. H. Al-Hassanieh and F.-H. Meisner. PO and GAL acknowledge financial support of FONDECYT (Chile) under grants 1080660 and 1100560. GBM and CAB acknowledge financial support by the National Science Foundation under Grant No. DMR-0710529, and AF acknowledges financial support from NSF Grant No. DMR-0955707. EV acknowledges support from CAPES, CNPq, and FAPEMIG (Brazil), and EVA acknowledges financial support of the Brazilian agencies FAPERJ (CNE) and CNPq (CIAM).

Appendix A: Canonical transformations

The system studied in this work consists of four different Fermi seas connected to a two-level CNT QD, schematically shown in Fig. 1(a). Canonical transformations, which eliminate part of the complexity of the problem,[40,41] can be performed over the system's Hamiltonian, given by Eqs. 2 to 4. In this Appendix, we briefly discuss these canonical transformations and how to calculate the Green's functions and the conductance.

1. Left-Right symmetry

The first transformation exploits the left-right symmetry. As a consequence of this symmetry (see Eq. 4), just the symmetric combination of left-right creation and annihilation operators in the α (β) band are coupled to the α (β) orbital of the CNT QD. This can be easily verified by simply rewriting Eq.4 as

$$H_{\rm hyb} = \sum_{\lambda;\lambda';\sigma} t_{\lambda\lambda'} \left[d^\dagger_{\lambda\sigma} (c_{\lambda' 1\sigma} + c_{\lambda' -1\sigma}) + H.c. \right], \tag{A1}$$

where λ and λ' can take values α or β.

Now, constructing the symmetric and anti-symmetric combinations of the $c_{\lambda\pm i\sigma}$ operators (where $\lambda = \alpha$ or β) for all $i \leq 1$, we can define a new basis composed of the following orthonormal states,

$$c^e_{\alpha i\sigma} = \frac{1}{\sqrt{2}} \left[c_{\alpha i\sigma} + c_{\alpha -i\sigma} \right], \tag{A2}$$

$$c^o_{\alpha i\sigma} = \frac{1}{\sqrt{2}} \left[c_{\alpha i\sigma} - c_{\alpha -i\sigma} \right], \tag{A3}$$

$$c^e_{\beta i\sigma} = \frac{1}{\sqrt{2}} \left[c_{\beta i\sigma} + c_{\beta -i\sigma} \right], \tag{A4}$$

$$c^o_{\beta i\sigma} = \frac{1}{\sqrt{2}} \left[c_{\beta i\sigma} - c_{\beta -i\sigma} \right]. \tag{A5}$$

Note that this change affects only the leads' fermion operators, keeping the CNT QD operators unchanged. In this new basis, the symmetric (even) combination will remain coupled to the CNT QD, while the anti-symmetric (odd) combination decouples from the system. The Hamiltonian $H_{\rm hyb}$ in this new basis takes the simple form,

$$H_{\rm hyb} = \sum_{\lambda;\lambda';\sigma} \sqrt{2}\, t_{\lambda\lambda'} \left[d^\dagger_{\lambda\sigma} c^e_{\lambda' 1\sigma} + H.c. \right]. \tag{A6}$$

Note that the couplings are now renormalized by a factor $\sqrt{2}$ (the factor 2 accounts for double-counting). It is easy to show that the band Hamiltonian $H_{\rm band}$ has its linear chain structure preserved under this transformation, as crossing terms between different chains cancel out. The system in this new basis is depicted in Fig. 1(b).

2. Using α-β Symmetry

As the CNT QD sits at the center of the system (equivalent to site 0) it is not affected by the previous transformation. Now we can take advantage of the α-β symmetry to simplify even more the problem. Note that under this new α-β transformation, the many-body terms will be also affected. The proposed transformation consists of using the symmetric and anti-symmetric

combinations between states $c^e_{\alpha i\sigma}$ and $c^e_{\beta i\sigma}$ [see Fig. 1(b)], and keeping the decoupled (odd) states untouched. The new basis for the even subspace will be (where now $i \geq 1$, i.e., i takes only positive values)

$$a_{i\sigma} = \frac{1}{\sqrt{2}}\left[c^e_{\alpha i\sigma} - c^e_{\beta i\sigma}\right], \tag{A7}$$

$$b_{i\sigma} = \frac{1}{\sqrt{2}}\left[c^e_{\alpha i\sigma} + c^e_{\beta i\sigma}\right], \tag{A8}$$

$$d_{+\sigma} = \frac{1}{\sqrt{2}}\left[d_{\alpha\sigma} + d_{\beta\sigma}\right], \tag{A9}$$

$$d_{-\sigma} = \frac{1}{\sqrt{2}}\left[d_{\alpha\sigma} - d_{\beta\sigma}\right], \tag{A10}$$

where the new operators $d_{+\sigma}$ and $d_{-\sigma}$ act on the α, β levels of the CNT QD. States associated to operators $d_{+\sigma}$ and $d_{-\sigma}$ are referred to as molecular orbitals (MO) in the main text. As in the previous transformation, the band Hamiltonian $H_{\rm band}$ retains its independent double-linear-chain structure in this case too. It is important to note that the total number of particles in the CNT QD is conserved under this transformation. For the special case $U' = U$, the many-body terms in the Hamiltonian $H_{\rm mb}$ just depend on the total number of particles. Therefore, its form will not change under this transformation:

$$H_{\rm mb} = \sum_{\sigma;\lambda=\pm} V_g n_{\lambda\sigma} + \frac{U}{2}\left[N_T^2 - N_T\right], \tag{A11}$$

where $N_T = \sum_\sigma (n_{+\sigma} + n_{-\sigma})$.

The Hamiltonian describing the connection between the CNT QD and the leads takes the form,

$$H_{\rm hyb} = \sum_\sigma \left[t_+\, d^\dagger_{+\sigma} a_{1\sigma} \;+\; t_-\, d^\dagger_{-\sigma} b_{1\sigma} + H.c.\right], \tag{A12}$$

where $t_\pm$ is given by Eqs. 5 and 6. An schematic of the effect of this transformation is shown in Fig. 1(c).

It is therefore easy to see that in the fully symmetric case ($t'' = t'$), and using that $t_- = \sqrt{2}\,(t' - t'')$, the MO $|-\rangle$ will be only capacitively coupled to the system, as $t_- = 0$. As mentioned in the main text, MO $|-\rangle$ is an electronic dark state. This effect is also known in the literature as Dicke effect or bound state in the continuous (BIC). In the absence of interactions ($U' = U = 0$) the MO $|-\rangle$ is completely decoupled from the charge reservoirs and appears as a delta resonance in the LDOS of the CNT QD, moving with V_g. For $U' = U \neq 0$, this state couples capacitively to MO $|+\rangle$ and contributes to an effective gate potential (acting on level $|+\rangle$) given by

$$V_g^* = V_g + U\, n_-, \tag{A13}$$

as explained in the main section of the manuscript.

For the sake of completeness, the many-body Hamiltoninan for the case $U' \neq U$ is provided in the $|\pm\rangle$ basis

$$H_{\rm mb} = H_1 + H_2 + H_3 + H_4 \tag{A14}$$

$$H_1 = \frac{U' + U}{2} \sum_{\lambda=+,-} \left(n_{\lambda\uparrow} n_{\lambda\downarrow} + n_{\lambda\uparrow} n_{\bar{\lambda}\downarrow}\right), \tag{A15}$$

$$H_2 = \frac{U' - U}{2} \sum_{\lambda=+,-} \left(c^\dagger_{\lambda\uparrow} c^\dagger_{\lambda\downarrow} c_{\bar{\lambda}\uparrow} c_{\bar{\lambda}\downarrow}\right), \tag{A16}$$

$$H_3 = \frac{U' - U}{4} \sum_{\lambda=+,-} \left(S^+_\lambda S^-_{\bar{\lambda}}\right), \tag{A17}$$

$$H_4 = U'\left(\, n_{+\uparrow}\, n_{-\uparrow} + \, n_{+\downarrow}\, n_{-\downarrow}\right). \tag{A18}$$

Note that, in the case $U' = U$, H_2 and H_3 vanish, and we recover Eq. A11. In addition, in the general case ($U' \neq U$), MOs $|\pm\rangle$ will not only be capacitively connected but also spin-spin correlated, with the character of the correlations (ferro or antiferro) being dependent on the relative values of U and U'. This points to a possibly very rich phase diagram, which will be fully studied in a forthcoming publication.[21]

3. Green's functions and conductance

In the main text, we studied this system using three different numerical techniques that require different formalisms to calculate the transport properties. We start by explaining how to calculate the conductance using LDECA.

In general, transport properties are related to Green's functions that propagate electrons from one lead to another (left to right, for example). For the system described in Fig. 1, the conductance can be written as,

$$G = 4\pi^2 \, |g_0|^2 \, t^4 \, [\rho_0(E_F)]^2, \tag{A19}$$

where

$$\begin{aligned} |g_0|^2 \;&=\; |G_{\alpha-1,\alpha 1}|^2 + |G_{\beta-1,\beta 1}|^2 \\ &\quad + |G_{\beta-1,\alpha 1}|^2 \; + |G_{\alpha-1,\beta 1}|^2, \end{aligned} \tag{A20}$$

and $G_{\lambda-1,\lambda' 1}$ stands for the Green function evaluated at the Fermi level E_F,

$$G_{\lambda-1,\lambda' 1} = \langle\langle c_{\lambda' 1}; c^{\dagger}_{\lambda-1}\rangle\rangle(\omega = E_F), \tag{A21}$$

where we keep the notation used in Eq. A2 for the creation/annihilation operators and the double bracket $\langle\langle;\rangle\rangle$ is the standard notation for Green's functions. Note that for simplicity we removed the spin subindex from the later equations. As our Hamiltonian does not have spin-flip terms, all terms in the propagators in this section have the same spin subindex and summation over repeated σ indexes is assumed.

Now we want to rewrite Eq. A19 using the canonical transformation given by Eqs. A2, to A5. By replacing in Eq. A21 the anti-transformation, we obtain two types of propagators,

$$G_{\lambda-1,\lambda 1} \;=\; \frac{1}{2}\left\{\langle\langle c^{e}_{\lambda 1}; {c^{e}_{\lambda 1}}^{\dagger}\rangle\rangle - \langle\langle c^{o}_{\lambda 1}; {c^{o}_{\lambda 1}}^{\dagger}\rangle\rangle\right\}, \tag{A22}$$

$$G_{\lambda-1,\lambda' 1} \;=\; \frac{1}{2}\,\langle\langle c^{e}_{\lambda' 1}; {c^{e}_{\lambda 1}}^{\dagger}\rangle\rangle. \tag{A23}$$

LDECA is a numerical technique where Green's functions can be easily evaluated. We solve, using LDECA, the system represented in Fig. 1(b). Then, using Eqs. A19, A20, A22, and A23, we can calculate the conductance as shown in Fig. 6.

We use two numerical techniques more, NRG and DMRG, but for the transport properties we limit these techniques to analyzing the case $t'' = t'$ ($\phi = \pi/4$). For this special case, we use all the symmetries of the system [see Fig. 1(c)]. Within NRG, we calculate the Green's function propagator at the MO $|+\rangle$. Then, using the equations of motion for Green's functions,[43] we left-right anti-transformation, obtaining the necessary propagators to evaluate Eqs. A19 and A20. For the DMRG technique we use a different approach. After the canonical transformations, using the left-right and α-β symmetries, we have that just MO $|+\rangle$ is connected to a reservoir. Using the fact that the system is a Fermi liquid, we can apply the Friedel sum rule, i.e., using the charge at the MO level $|+\rangle$, the conductance can be calculated by the equation[42]

$$G = 2G_0 \, \sin^2\left(\frac{\pi \, n_+}{2}\right). \tag{A24}$$

This procedure cannot be used if $\phi \neq \pi/4$, the conductance cannot be calculated as just described. However, the occupancy of the CNT qD levels α and β, as well as MO $|+\rangle$ and $|-\rangle$, can still be evaluated using DMRG.

Appendix B: Non interacting case

In the absence of interactions ($U = 0$), the physical properties of the system described in Fig. 1, as for instance, the local density of states (LDOS) and the conductance, can be calculated exactly.

We can start by analyzing the LDOS at each level of the QD. As we mentioned in Appendix A a canonical transformation can be performed mixing levels α and β of the QD into two new levels, a symmetric MO $|+\rangle$ and an anti-symmetric MO $|-\rangle$. The LDOS at any of the AO levels of the QD can be calculated as the superposition of the LDOS at MO $|+\rangle$ and MO $|-\rangle$ (since $\rho_\alpha = \rho_\beta$),

$$\rho_\lambda(\omega) = \frac{\rho_+(\omega) + \rho_-(\omega)}{2}, \tag{B1}$$

with $\lambda = \alpha$ or β.

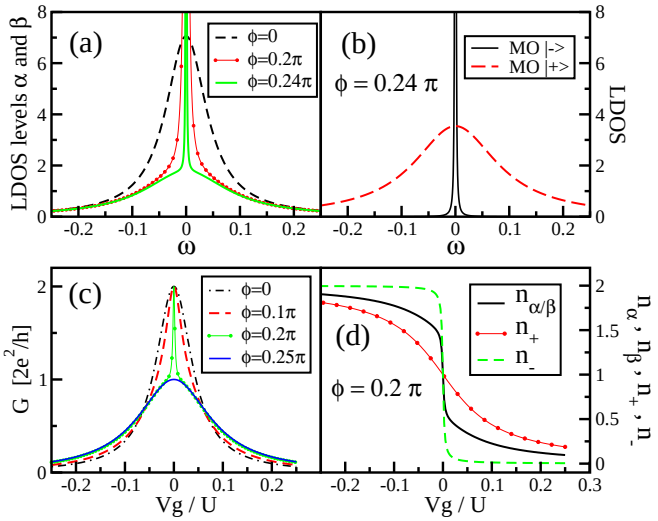

FIG. 9: (Color online) (a) LDOS of levels α and β for $V_g = 0$, $t_0 = 0.15$, and different values of ϕ. When $\phi \to \pi/4$, MO $|-\rangle$ gradually decouples from the band and a sharp resonant state develops at V_g in the LDOS. (b) LDOS for MOs $|\pm\rangle$ for $\phi = 0.24\pi$. (c) Conductance as a function of V_g calculated for $t_0 = 0.15$ and different values of ϕ. When $\phi = \pi/4$ the MO $|-\rangle$ is totally decoupled and the conductance reduces by half, indicating that just one channel is active. (d) Charging of levels α, β, and MOs $|\pm\rangle$ as a function of V_g for the case $\phi = 0.2\pi$. As MO $|-\rangle$ is weakly coupled, its charging resembles a step function.

For $U = U' = 0$, MOs $|+\rangle$ and $|-\rangle$ are totally independent. Their LDOS is associated to the corresponding coupling with the contacts. Each of these levels will have a width given by

$$\Gamma_\delta(\omega) = \pi {t_\delta}^2 \rho_0(\omega), \tag{B2}$$

where δ stands for $|+\rangle$ or $|-\rangle$ and ρ_0 is the LDOS at the leads. As shown above, in the main text and in Appendix A, when $\phi \to \pi/4$, the anti-symmetric state gradually decouples from the charge reservoir (as $t_- \to 0$) and its LDOS becomes a delta function. When $\phi = \pi/4$ the MO $|-\rangle$ is completely decoupled and $\rho_\alpha = \rho_\beta$ is a superposition of a delta function and a resonant peak with width Γ_+. A similar effect can be observed in other DQD systems[23,27] or in a double Rashba ring[24].

Figure 9(a) shows ρ_α and ρ_β for different values of ϕ. The LDOS was calculated using the Green's function equations of motion formalism, which is exact in the limit of $U = 0$. Fig. 9(b) shows the LDOS for the MOs $|+\rangle$ and $|-\rangle$ for $\phi = 0.24\pi$ and $V_g = 0.0$. For this value of ϕ, close to $\pi/4$, the MO $|-\rangle$ is almost decoupled and therefore appears as a narrow resonance located at V_g.

The formula for the conductance is given by[42]

$$G(V_g) = 2G_0 \frac{\tilde{t_0}[t^2 V_g^2(1+\sin^2 2\phi) + \tilde{t_0}\cos^4 2\phi]}{T_+(V_g)\ T_-(V_g)}, \tag{B3}$$

$$T_\pm(V_g) = \tilde{t_0}(1 \pm \sin 2\phi)^2 + t^2 V_g^2, \tag{B4}$$

where $G_0 = 2e^2/h$ and $\tilde{t_0} = 4t_0^4$.

When levels α and β are not mixed ($t'' = 0$, i.e., $\phi = 0$), we can see that the maximum of the conductance occurs for $V_g = 0$, taking the value $G = 2G_0$, indicating that both channels are active.

As seen above, for $\phi = \pi/4$, one of the channels is decoupled and the maximum of the conductance is G_0. For values of ϕ close to $\pi/4$ Eq.B4 can be written as a superposition of two Breit-Wigner line shapes,[26,27]

$$G(\phi \sim \pi/4) \sim G_0 \left(\frac{\lambda_+^2}{V_g^2 + \lambda_+^2} + \frac{\lambda_-^2}{V_g^2 + \lambda_-^2} \right), \tag{B5}$$

where

$$\lambda_+ = 4t_0^2/t, \tag{B6}$$

$$\lambda_- = 2t_0^2/t\ [1 - \sin 2\phi]\,. \tag{B7}$$

Using Dicke effect terminology, the first term in Eq. B5 corresponds to the contribution of the super-radiant state (symmetric channel $|+\rangle$) with a width λ_+, and the second term corresponds to the sub-radiant state (anti-symmetric channel $|-\rangle$) with a width λ_-.

In Fig. 9(c) we show the conductance for different values of ϕ. For $\phi = 0$ both channels are active and have the same width. By increasing ϕ, the MO $|-\rangle$ starts to decouple and this is reflected in a narrower line in the conductance superposed on the wider line given by MO $|+\rangle$. When $\phi = \pi/4$ the MO $|-\rangle$ is completely decoupled and does not give any contribution to the conductance, whose maximum is reduced from $2G_0$ to G_0.

Panel (d) of Fig. 9 shows the charging for the case $\phi = 0.2\pi$. Note that the charging of MO $|-\rangle$ is almost a step function. When $\phi = \pi/4$, the charging of levels α and β will occur discontinuously.

---

* Corresponding author: martins@oakland.edu

[1] R. Saito, G. Dresselhaus, and M. S. Dresselhaus, *Physical Properties of Carbon Nanotubes* (Imperial College Press, London 1998).

[2] S. J. Tans, A. R. M. Verschueren, and C. Dekker, Nature **393**, 49 (1998).

[3] T. Rueckes, K. Kim, E. Joselevich, G. Y. Tseng, C. L. Cheung, and C. M. Lieber, Science **289**, 94 (2000).

[4] A. C. Hewson, *The Kondo Effect to Heavy Fermions* (Cambridge University Press, Cambridge 1993).

[5] J. Nygård, D. H. Cobden, and P. E. Lindelof, Nature **480**, 342 (2000).

[6] P. Jarillo-Herrero, J. Kong, H. S. J. van der Zant, C. Dekker, L. P. Kouwenhoven, and S. DeFranceschi, Nature **434**, 484 (2005); A. Makarovski, A. Zhukov, J. Liu, and G. Finkelstein, Phys. Rev. B **75**, 241407(R) (2007); A. Makarovski, J. Liu, and G. Finkelstein, Phys. Rev. Lett. **99**, 066801 (2007).

[7] M. S. Choi, R. Lopez, and R. Aguado, Phys. Rev. Lett. **95**, 067204 (2005); M. R. Galpin, D. E. Logan, and H. R. Krishnamurthy, J. Phys.: Condens. Matter **18**, 6545 (2006); **18**, 6571 (2006).

[8] M. R. Galpin, D. E. Logan, and H. R. Krishnamurthy, Phys. Rev. Lett. **94**, 186406 (2005).

[9] J. S. Lim, M.-S. Choi, M. Y. Choi, R. Lopez, and R. Aguado, Phys. Rev. B **74**, 205119 (2006).

[10] C. A. Büsser and G. B. Martins, Phys. Rev. B **75**, 045406 (2007).

[11] M. Mizuno, E. H. Kim, and G. B. Martins, J. Phys.: Condens. Matter **21**, 292203 (2009).

[12] I. H. Chan, R. M. Westervelt, K. D. Maranowski, and A. C. Gossard, Appl. Phys. Lett. **80**, 1818 (2002); A. W. Holleitner, R. H. Blick, and K. Eberl, *idem* **82**, 1887 (2003); D. T. McClure, L. DiCarlo, Y. Zhang, H.-A. Engel, C. M. Marcus, M. P. Hanson, and A. C. Gossard, Phys. Rev. Lett. **98**, 056801 (2007); A. Hübel, K. Held, J. Weis, and K. v. Klitzing, *idem* **101**, 186804 (2008); T. Hatanoa, S. Amaha, T. Kubo, S. Teraoka, Y. Tokura, J. A. Gupta, D. G. Austing, and S. Tarucha, arXiv:1008.0071v1.

[13] U. Wilhelm, J. Schmid, J. Weis, and K. v. Klitzing, Physica E **14** 385 (2002).

[14] R. Bulla, T. A. Costi, and T. Pruschke, Rev. Mod. Phys. **80**, 395 (2008).

[15] S. R. White, Phys. Rev. Lett. **69**, 2863 (1992).

[16] E. V. Anda, G. Chiappe, C. A. Büsser, M. A. Davidovich, G. B. Martins, F. Heidrich-Meisner, and E. Dagotto, Phys. Rev. B **78**, 085308 (2008).

[17] G. B. Martins and C. A. Büsser, Physica B **403**, 1514 (2008).

[18] G. B. Martins, private communication.

[19] For an example of this change to molecular orbitals, please see E. Vernek, C. A. Büsser, G. B. Martins, E. V. Anda, N. Sandler, and S. E. Ulloa, Phys. Rev. B **80**, 035119 (2009).

[20] F. D. M. Haldane, Phys. Rev. Lett. **40**, 416 (1978).

[21] Results for a model where inter- and intra-orbital repulsion terms are different will be presented elsewhere.

[22] P. A. Orellana, M. L. Ladrón de Guevara, F. Claro, Phys. Rev. B **70**, 233315 (2004).

[23] P. A. Orellana, G. A. Lara, and E. V. Anda, Phys. Rev. B **74**, 193315 (2006).

[24] V. M. Apel , P. A. Orellana and M. Pacheco, Nanotech. **19**, 355202 (2008).

[25] M. L. Ladrón de Guevara, P. A. Orellana, Phys. Rev. B **73**, 205303 (2006).

[26] B. Solís, M. L. Ladrón de Guevara, P. A. Orellana, Phys. Lett. A **372**, 4736 (2008).

[27] M. L. Ladrón de Guevara, F. Claro, P. A. Orellana, Phys. Rev. B **67**, 195335 (2003).

[28] R. H. Dicke, Phys. Rev. 89, 472 (1953).

[29] K. Chen and C. Jayaprakash, Phys. Rev. B **52**, 14436 (1995).

[30] The NRG calculations for very large values of U/Γ (panels (a) and (b) of Fig. 3, with $U/\Gamma = 400$ and 100, respectively) are too computationally demanding and the authors did not achieve the desired convergence.

[31] Note that in eqs. (A14) to (A18) one sees that, in the MO basis, and for $U \neq U'$, one has a Heisenberg term ($\overrightarrow{S}_+ \cdot \overrightarrow{S}_-$) between the MOs (this can be easily obtained after some straightforward algebra). As discussed in M. Vojta, R. Bulla, and W. Hofstetter, Phys. Rev. B **65**, 140405 (2002) and G. Zarand, C.-H. Chung, P. Simon, and M. Vojta, Phys. Rev. Lett. **97**, 166802 (2006), this term leads to a two stage Kondo (TSK) effect (see also Ref. 16 for an LDECA calculation involving a system displaying a TSK regime). Notice that $U \neq U'$ leads to other terms in the many-body MO Hamiltonian, whose effect should also be taken in account. This will be done in detail in a future publication.

[32] Results for different values of t''/t' can be seen in Fig. 3 of ref. 17. Note that those results are for a different regime than the ones presented here (they are located between the Kondo and Intermediate Valence regimes, while some of the present results are deeper into the Kondo regime). Note also that, as t'' varies, Γ was not kept constant in those calculations.

[33] C. Karrasch, T. Hecht, A. Weichselbaum, J. von Delft, Y. Oreg, and V. Meden, New Journ. Phys. **9**, 123 (2007).

[34] An analysis of the variation with V_g of the eigenvalues of $H_{\rm mb}$ [eq. (3)] shows that $V_g/U = -1.0$ marks the degeneracy between the ground states of sectors with one and two electrons (CB point), conducive to strong charge fluctuations and sequential tunneling.
[35] G. B. Martins, C. A. Büsser, K. A. Al-Hassanieh, A. Moreo, and E. Dagotto, Phys. Rev. Lett. **94**, 026804 (2005).
[36] See G.-H. Ding, F. Ye, and B. Dong, J. Phys.: Condens. Matter **21** 455303 (2009), and references therein.
[37] Based on that, the authors would feel tempted to loosely refer to T_0 as the 'many-body energy'. We refrain from that though, as we feel that the definition of T_0 and its calculation have to first be refined and better understood.
[38] D. Goldhaber-Gordon, J. Göres, M. A. Kastner, Hadas Shtrikman, D. Mahalu, and U. Meirav, Phys. Rev. Lett. **81**, 5225 (1998).
[39] Computational efforts are underway to explore the accuracy and physical information contained in this simple definition of T_0.
[40] B. A. Jones, C. M. Varma, Phys. Rev. Lett. **58**, 843 (1987). K. Ingersent, B. A. Jones, and J. W. Wilkins, Phys. Rev. Lett. **69**, 2594 (1992).
[41] A. Oguri, S. Amaha, Y. Nishikawa, T. Numata, M. Shimamoto, A. C. Hewson, S. Tarucha, arXiv:1008.1821.
[42] E. V. Anda, F. Flores, J. Phys.: Condens. Matter **3**, 9087 (1991). Y. Meir, N. S. Wingreen, Phys. Rev. Lett. **68**, 2512 (1992).
[43] D. N. Zubarev, Usp. Fiz. Nauk. **71**, 71 (1960) [English transl.: Soviet Phys. Usp. **3**, 320 (1960)]. J. W. Negele and H. Orland, *Quantum Many-Particle Systems* (Perseus Books, Reading, MA, 1998).